

# Two Photon Radiation in $W$ and $Z$ Boson Production at the Tevatron Collider

U. Baur\*

*Department of Physics, State University of New York, Buffalo, NY 14260, USA*

T. Stelzer†

*Department of Physics, University of Illinois, 1110 West Green Street, Urbana, IL 61801, USA*

## Abstract

We present a calculation of two photon radiation in  $W$  and  $Z$  boson production in hadronic collisions, based on the complete matrix elements for the processes  $q\bar{q}' \rightarrow \ell^\pm \nu \gamma \gamma$  and  $q\bar{q} \rightarrow \ell^+ \ell^- \gamma \gamma$ , including finite charged lepton masses. In order to achieve stable numerical results over the full phase space, multiconfiguration Monte Carlo techniques are used to map the peaks in the differential cross section. Numerical results are presented for the Fermilab Tevatron.

---

\*e-mail: baur@ubhex.physics.buffalo.edu

†e-mail: tstelzer@uiuc.edu

## I. INTRODUCTION

The Standard Model of electroweak interactions (SM) so far has met all experimental challenges and is now tested at the 0.1% level [1]. However, there is little direct experimental information on the mechanism which generates the masses of the weak gauge bosons. In the SM, spontaneous symmetry breaking is responsible for mass generation. The existence of a Higgs boson is a direct consequence of this mechanism. At present the negative result of direct searches performed at LEP2 imposes a lower bound of  $M_H > 98.8$  GeV [2] on the Higgs boson mass. Indirect information on the mass of the Higgs boson can be extracted from the  $M_H$  dependence of radiative corrections to the  $W$  boson mass,  $M_W$ , and the effective weak mixing angle,  $\sin^2 \theta_{eff}^{lept}$ . Assuming the SM to be valid, a global fit to all available electroweak precision data yields a (one-sided) 95% confidence level (CL) upper limit on  $M_H$  of about 260 GeV [1–3].

Future more precise measurements of  $M_W$  and the top quark mass,  $m_{top}$ , will lead to more accurate information on the Higgs boson mass [4–6]. Currently, the  $W$  boson mass is known to  $\pm 42$  MeV [7] from direct measurements. The uncertainties of the individual experiments contributing to this value are between about 80 MeV and 110 MeV [7,8]. The present uncertainty of the top quark mass from direct measurements is  $\pm 5.1$  GeV [9]. With a precision of 30 MeV (10 MeV) for the  $W$  mass, and 2 GeV for the top quark mass,  $M_H$  can be predicted from a global analysis with an uncertainty of about 30% (15%) [5,6]. Comparison of these indirect constraints on  $M_H$  with the results from direct Higgs boson searches at LEP2, the Tevatron collider, and the Large Hadron Collider (LHC) will be an important test of the SM. They will also provide restrictions on the parameters of the Minimal Supersymmetric extension of the Standard Model (MSSM) [10].

A significant improvement in the  $W$  mass uncertainty is expected in the near future from measurements at LEP2 [11] and the Fermilab Tevatron  $p\bar{p}$  collider [5]. The ultimate precision expected for  $M_W$  from the combined LEP2 experiments is 30 – 40 MeV [11]. At the Tevatron, integrated luminosities of order  $2 \text{ fb}^{-1}$  are envisioned in the Main Injector

Era (Run II), and one expects to measure the  $W$  mass with a precision of approximately 40 MeV [5] per experiment. The prospects for a precise measurement of  $M_W$  would further improve if a significant upgrade in luminosity beyond the goal of the Main Injector could be realized. With recent advances in accelerator technology [12], Tevatron collider luminosities of order  $10^{33} \text{ cm}^{-2} \text{ s}^{-1}$  may become a reality, resulting in integrated luminosities of up to  $10 \text{ fb}^{-1}$  per year. With a total integrated luminosity of  $30 \text{ fb}^{-1}$ , one can target a precision of the  $W$  mass of 15 – 20 MeV [5]. A similar or better accuracy may also be reached at the LHC [13].

In order to measure the  $W$  boson mass with high precision in a hadron collider environment, it is necessary to fully understand and control higher order QCD and electroweak (EW) corrections to  $W$  production. The determination of the  $W$  mass in a hadron collider environment requires a simultaneous precision measurement of the  $Z$  boson mass,  $M_Z$ , and width,  $\Gamma_Z$ . These quantities serve as reference points. When compared to the value measured at LEP, they help to accurately determine the energy scale and resolution of the electromagnetic calorimeter, and to constrain the muon momentum resolution [5]. In order to extract  $M_W$  from hadron collider data, it is therefore also necessary to understand the higher order QCD and EW corrections to  $Z$  boson production in hadronic collisions.

Electroweak radiative corrections have a significant impact on the  $W$  and  $Z$  boson masses and widths extracted from experiment. Recent improved calculations of the  $\mathcal{O}(\alpha)$  EW corrections to  $W$  production [14], and of the  $\mathcal{O}(\alpha)$  QED corrections to  $Z$  production in hadronic collisions [15], have shown that the main effect is caused by final state photon radiation. When detector effects are included,  $\mathcal{O}(\alpha)$  radiative corrections shift the  $W$  mass by about  $-50$  MeV in the electron case, and approximately  $-160$  MeV in the muon case [16,17]. The effect on the  $Z$  mass is about a factor two larger than that on  $M_W$  for both electron and muon final states.  $\mathcal{O}(\alpha)$  photon emission also shifts the width of the  $W$  boson extracted from the tail of the transverse mass distribution by approximately  $-70$  MeV [18]. The size of the shift in  $M_W$ ,  $M_Z$  and the  $W$  width introduced by the  $\mathcal{O}(\alpha)$  corrections raises the question of how strongly  $\mathcal{O}(\alpha^2)$  corrections affect these quantities.

In order to reliably calculate the impact of the  $\mathcal{O}(\alpha^2)$  corrections to  $p\bar{p} \rightarrow W^\pm \rightarrow \ell^\pm\nu$  and  $p\bar{p} \rightarrow \gamma^*, Z \rightarrow \ell^+\ell^-$  ( $\ell = e, \mu$ ) on the  $W$  and  $Z$  masses extracted from experiment, a full calculation including real and virtual corrections, which is valid over the entire allowed phase space, is needed. So far, only partial calculations for the  $\mathcal{O}(\alpha^2)$  real photon corrections,  $p\bar{p} \rightarrow W^\pm \rightarrow \ell^\pm\nu\gamma\gamma$  and  $p\bar{p} \rightarrow \gamma^*, Z \rightarrow \ell^+\ell^-\gamma\gamma$  exist [19,20]. In Ref. [19] the structure function approach for photon radiation is used to perform the calculation and, therefore, only final state photon radiation in the leading log approximation is included. The results obtained using this approach are reliable only for small opening angles between the photons and the charged leptons. The calculation of Ref. [20] is based on the full set of tree level Feynman diagrams contributing to  $\ell\nu\gamma\gamma$  and  $\ell^+\ell^-\gamma\gamma$  production. In addition, to preserve gauge invariance when finite  $W$  width effects are included, the imaginary part of the  $WW\gamma$  and  $WW\gamma\gamma$  one-loop vertex corrections is taken into account. However, charged leptons are assumed to be massless, and thus a finite lepton – photon separation cut has to be imposed in order to avoid the collinear singularities associated with final state radiation.

The first step towards a calculation of the  $\mathcal{O}(\alpha^2)$  corrections to  $W$  and  $Z$  boson production in hadronic collisions thus is to perform a calculation of  $\ell\nu\gamma\gamma$  and  $\ell^+\ell^-\gamma\gamma$  production which

- is based on the full set of Feynman diagrams contributing at tree level,
- includes finite lepton mass effects,
- is gauge invariant when finite  $W$  width effects are taken into account,
- and is valid for arbitrary lepton – photon opening angles.

In addition, in order to obtain reliable information on the shift in  $M_W$  and  $M_Z$  caused by two photon radiation, the numerical calculation should be stable for photon energies as small as the tower threshold of the electromagnetic calorimeter of the Tevatron experiments, which is of  $\mathcal{O}(100 \text{ MeV})$ . In this paper we present such a calculation.

While the calculation of the  $q\bar{q} \rightarrow \ell^+\ell^-\gamma\gamma$  and  $q\bar{q}' \rightarrow \ell\nu\gamma\gamma$  matrix elements is straightforward, the phase space integration presents some challenges, due to the sharp peaks in the matrix elements which arise from the soft and collinear singularities. The collinear singularities associated with final state radiation are regulated by the finite mass of the leptons whereas soft and initial state collinear singularities are rendered finite by transverse momentum cuts imposed on the photons. Both soft and collinear singularities produce large contributions to the cross section in small regions of phase space. Standard adaptive Monte Carlo integration routines such as VEGAS [21] do not yield a numerically stable result of the cross section for processes which exhibit a complicated peaking structure in the matrix elements. To obtain numerically stable and accurate results for such processes, a multi-channel Monte Carlo approach [22], augmented by the adaptive weight optimization procedure described in Ref. [23], is frequently used. The disadvantage of the multi-channel Monte Carlo approach is that the peaks in the matrix elements have to be mapped by hand, thus requiring a substantial amount of analytic work which has to be repeated for each new process one wishes to analyze.

Our calculation is based on a similar approach which adds the benefit of largely automizing the mapping of the peaks in the matrix elements. The process independent features of our approach, and the resulting multiconfiguration Monte Carlo (MCMC) integration program, are briefly described in Sec. II. Full details will be given elsewhere [24]. In Sec. III we discuss technical details associated with the calculation of the  $q\bar{q} \rightarrow \ell^+\ell^-\gamma\gamma$  and  $q\bar{q}' \rightarrow \ell\nu\gamma\gamma$  matrix elements and present numerical results for two photon radiation in  $W$  and  $Z$  events at the Tevatron collider ( $p\bar{p}$  collisions at 1.8 TeV). Finally, summary remarks are given in Sec. IV.

## II. PHASE SPACE INTEGRATION

The matrix elements for  $q\bar{q} \rightarrow \ell^+\ell^-\gamma\gamma$  and  $q\bar{q}' \rightarrow \ell\nu\gamma\gamma$  have many sharply peaked regions throughout phase space. In addition to the Breit-Wigner resonances around the  $W$  or  $Z$  pole

and a pole at small  $\ell^+\ell^-$  invariant masses due to photon exchange, there are singularities when either photon becomes soft, or collinear with a charged particle. Although these soft and collinear singularities are regulated by energy or transverse momentum cuts and fermion masses, they result in large contributions to the cross section over relatively small regions of phase space and cause difficulties for standard integration techniques.

Integrating over the parton distributions and final state momenta in general requires performing a  $(3N_{final}-4)+2$  dimensional integral over a phase space which may include many cuts. Here  $N_{final}$  is the number of particles in the final state. If the number of dimensions is large, the integral is most easily carried out using Monte Carlo techniques. Monte Carlo integration approximates the integral by taking the average of a number of points,  $N$ , selected at random, and multiplying by the volume,  $V$ , over which one is integrating,

$$\int f(x)dx \simeq \frac{1}{N} \sum_i f(x_i) \times V. \quad (1)$$

Provided the function  $f(x)$  which is to be integrated is sufficiently flat, the number of points for convergence is independent of the number of dimensions. However, if  $f(x)$  is sharply peaked convergence may be exponentially slow.

In order to use Monte Carlo techniques for integrating a sharply peaked function, it is necessary to remove the peaks. Peaks which are analytically integrable, and for which the integral is invertible, can be smoothed with the appropriate transformation of variables. A Breit-Wigner resonance is an excellent example for such a case. The transformation  $y = \arctan(x)$  removes the peak and makes the integrand flat. Collinear and soft poles often require more involved transformations which may not have general analytical solutions.

Adaptive Monte Carlo programs such as VEGAS are able to flatten peaks by using numeric approximations of the integrand. The result is not as fast, or efficient as analytically removing the peaks, however it is more convenient. For most applications this is very desirable. The major restriction is that programs such as VEGAS can only remove peaks which are in the plane of one of the integration variables. For example, these programs will successfully flatten the peaks in the function

$$f(x, y) = \frac{1}{x} \frac{1}{y} , \quad (2)$$

but they will not be able to flatten those for

$$f(x, y) = \frac{1}{x+y} \frac{1}{x-y} , \quad (3)$$

unless a change of variables is performed. For processes with relatively few peaks, it is usually possible to map each peak to one of the integration variables. For complicated process such as  $q\bar{q} \rightarrow \ell^+\ell^-\gamma\gamma$  and  $q\bar{q}' \rightarrow \ell\nu\gamma\gamma$ , this is not the case.

In cases where it is not possible to simultaneously map every peak to an integration variable, there are two classes of solutions available. The first is to divide up phase space with cuts, such that the peaks in each region can be mapped to the integration variables. An adaptive Monte Carlo integration routine is used for each region separately. The results from each region are combined to obtain the total cross section. This method is effective for processes with relatively simple peaking structure, however as the number of peaks increases the technique quickly becomes cumbersome and prone to error.

The second technique [22,23] is to choose points in phase space not according to a single distribution, but according to the sum of multiple distributions. Each distribution is responsible for a specific set of peaks. The optimal number of points from each distribution is chosen using an algorithm which minimizes the Monte Carlo integration error [23]. With each channel, a different set of poles is analytically removed. The resulting code is very fast and efficient, however it requires significant analytic work, which must be repeated for each new process.

In our approach, we have combined the power of multichannel integration with the convenience offered by adaptive Monte Carlo integration routines such as VEGAS. The result is a general and flexible multiconfiguration Monte Carlo program called MCMC which can numerically integrate sharply peaked functions in many dimensions with minimal input from the user.

Feynman diagrams offer a convenient mechanism for determining in which dimensions peaks may appear. At tree level strong peaks in the cross section are always associated with

a propagator going on-shell. We have implemented a general phase-space generator based on Feynman diagrams. Given a tree-level Feynman diagram, it maps a set of random numbers to a point in phase space such that each propagator represents one of the dimensions of integration. The operation is invertible so it can also return the set of random numbers associated with any point in phase space. The user specifies the momentum flow of the contributing Feynman diagrams in a simple include file, together with the masses and widths of the Breit-Wigner resonances which appear in each diagram. All other aspects of the phase space integration are handled automatically by the program. A more detailed description of the approach will be given elsewhere [24].

The convenience of MCMC is best illustrated in a simple example. Consider the process  $\nu_\mu \bar{\nu}_\mu \rightarrow e^+ e^- \gamma \gamma$  for a center of mass energy of  $\sqrt{s} = 100$  GeV, where each of the final state particles is required to have a transverse momentum  $p_T > 10$  GeV. The electron mass is assumed to be variable. The six Feynman diagrams associated with this process can easily be generated with a program such as MadGraph [25]. The diagrams generated by MadGraph are shown in Fig. 1. Each diagram represents a phase space configuration in the MCMC code with the appropriate poles mapped to the integration variables.

These configurations are input to the integration package, which then searches for peaks, and determines the optimal number of points to choose from each configuration using an algorithm which minimizes the integration error. Table I compares the cross sections obtained using the traditional single configuration approach with those from MCMC as the electron mass is varied from 0.01 GeV to 10 GeV. Notice that for large masses, the matrix element is relatively flat and a single configuration accurately integrates the cross section. However, as the electron mass decreases, the contribution from the collinear regions becomes increasingly important, and the single configuration package is unable to accurately integrate the function. Not only is the error larger, but even with  $5 \times 10^6$  integration points, the single configuration integration is giving the wrong result as it samples all of the points from the peaks it has mapped to integration variables, completely neglecting the peaks which are only sampled by the other configurations. Due to the mass singular terms associated



with final state radiation in the collinear limit, the cross section scales approximately with  $(\log(m_e^2/s))^2$  for small electron masses,  $m_e \leq 1$  GeV. This provides a simple check on the accuracy of the MCMC result.

The primary difference between our approach and other multichannel techniques is its generality. The mapping of uniformly distributed random numbers to points in phase space can be broken down into two steps. First the uniformly distributed random numbers are deformed into non-uniform numbers, with a corresponding Jacobian. Next these non-uniform numbers are mapped to four-momenta in phase space with another Jacobian. For each step, one can choose to perform an analytic transformation which will be very efficient for the particular process being studied, or one can choose a general transformation which is not optimized for the specific process, but will work for any process. The approach of Ref. [23] produces highly optimized code for both transformations. In Ref. [26], a general procedure for the transformation from uniform space to a deformed space is given, but optimized procedures for the transformation to phase space are chosen. The MCMC program provides general algorithms for both transformations, similar to the approach used by CompHEP [27,28] to perform the phase space integration. The resulting code is in general slightly slower than that resulting from the other two approaches, however we believe its user friendliness makes up for this short coming. The advantage of user friendly programs at the expense of computer time has already been demonstrated by packages such as MadGraph, CompHEP [27,29] and GRACE [29] which quickly produce non-optimized tree-level matrix elements. Indeed the synthesis of the integration package outlined here with automatically generated matrix elements will allow the user to concentrate on the physics issues rather than numerical integration techniques. While MCMC naturally interfaces with MadGraph and HELAS [30], matrix elements resulting from any other automated or non-automated calculation can be used.

### III. $\ell\nu\gamma\gamma$ AND $\ell^+\ell^-\gamma\gamma$ PRODUCTION AT THE FERMILAB TEVATRON

We shall now discuss the calculation of  $\ell\nu\gamma\gamma$  and  $\ell^+\ell^-\gamma\gamma$  production in hadronic collisions, together with some phenomenological applications relevant for future  $W$  mass measurements at hadron colliders. To calculate the matrix elements for  $q\bar{q} \rightarrow \ell^+\ell^-\gamma\gamma$  and  $q\bar{q}' \rightarrow \ell^\pm\nu\gamma\gamma$  we use MadGraph which automatically generates the SM matrix elements in HELAS format. When photon exchange is taken into account, 40 Feynman diagrams contribute to  $\ell^+\ell^-\gamma\gamma$  production, while there are 21 diagrams for  $\ell^\pm\nu\gamma\gamma$  production. Taking into account symmetries in the phase space mapping, 20 (12) different configurations contribute to  $q\bar{q} \rightarrow \ell^+\ell^-\gamma\gamma$  ( $q\bar{q}' \rightarrow \ell\nu\gamma\gamma$ ).

In order to maintain electromagnetic gauge invariance for  $q\bar{q}' \rightarrow \ell^\pm\nu\gamma\gamma$  in presence of finite  $W$  width effects, the  $W$  propagator and the  $WW\gamma$  and  $WW\gamma\gamma$  vertex functions in the amplitudes generated by MadGraph have to be modified [20,31]. Finite width effects are included by resumming the imaginary part of the  $W$  vacuum polarization,  $\Pi_W(q^2)$ . The transverse part of  $\Pi_W(q^2)$  receives an imaginary contribution

$$\text{Im } \Pi_W^T(q^2) = q^2 \frac{\Gamma_W}{M_W} \quad (4)$$

while the imaginary part of the longitudinal piece vanishes. The  $W$  propagator is thus given by

$$D_W^{\mu\nu}(q) = \frac{-i}{q^2 - M_W^2 + iq^2\gamma_W} \left[ g^{\mu\nu} - \frac{q^\mu q^\nu}{M_W^2} (1 + i\gamma_W) \right], \quad (5)$$

with

$$\gamma_W = \frac{\Gamma_W}{M_W}, \quad (6)$$

where  $\Gamma_W$  denotes the  $W$  width. A gauge invariant expression for the amplitude is then obtained by attaching the final state photons to all charged particle propagators, including those in the fermion loops which contribute to  $\Pi_W(q^2)$ . As a result, the lowest order  $WW\gamma$  and  $WW\gamma\gamma$  vertex functions,  $\Gamma_0^{\alpha\beta\mu}$  and  $\Gamma_0^{\alpha\beta\mu\rho}$ , are modified [20,31] to

$$\Gamma^{\alpha\beta\mu} = \Gamma_0^{\alpha\beta\mu}(1 + i\gamma_W), \quad (7)$$

$$\Gamma^{\alpha\beta\mu\rho} = \Gamma_0^{\alpha\beta\mu\rho}(1 + i\gamma_W). \quad (8)$$

The SM parameters used in our numerical calculations are  $M_W = 80.3$  GeV,  $\Gamma_W = 2.046$  GeV,  $M_Z = 91.19$  GeV,  $\Gamma_Z = 2.49$  GeV, and  $\alpha(M_Z^2) = 1/128$ . These values are consistent with recent measurements at LEP, LEP2, the SLC and the Tevatron [7]. We use the parton distribution functions set A of Martin-Roberts-Stirling [32] with the factorization scale set equal to the parton center of mass energy  $\sqrt{\hat{s}}$ . All numerical results are obtained for  $p\bar{p}$  collisions with a center of mass energy of  $\sqrt{s} = 1.8$  TeV. In Run II, the Tevatron collider is foreseen to operate at  $\sqrt{s} = 2$  TeV. For a center of mass energy of 2 TeV, results qualitatively similar to those reported here are obtained. Cross sections are about 5% higher than those found for  $\sqrt{s} = 1.8$  TeV. Since the total cross sections for  $\ell^+\nu\gamma\gamma$  and  $\ell^-\nu\gamma\gamma$  production are equal in  $p\bar{p}$  collisions, we shall not consider the  $\ell^-\nu\gamma\gamma$  channel in the following.

To simulate the fiducial and kinematic acceptances of detectors, we impose the following transverse momentum ( $p_T$ ) and pseudo-rapidity ( $\eta$ ) cuts on electrons and muons:

electrons	muons
$p_T(e) > 20$ GeV	$p_T(\mu) > 25$ GeV
$ \eta(e)  < 2.5$	$ \eta(\mu)  < 1.0$
$\cancel{p}_T > 20$ GeV	$\cancel{p}_T > 25$ GeV

Here,  $\cancel{p}_T$  denotes the missing transverse momentum which we identify with the transverse momentum of the neutrino in  $\ell\nu\gamma\gamma$  production. The  $\cancel{p}_T$  cut is only applied in  $\ell\nu\gamma\gamma$  production. The cuts listed above approximately model the acceptance of the CDF detector for electrons and muons in Run I. Qualitatively similar numerical results are obtained if cuts are used which approximate the phase space region covered by the upgraded CDF detector for Run II [33], or if cuts are used which model the acceptance of the DØ detector [34].

In addition to the lepton cuts listed above, a pseudo-rapidity cut

$$|\eta(\gamma)| < 3.6, \quad (9)$$

and a transverse momentum cut on the photons are imposed. In order to be able to accurately determine the shift in the  $W$  and  $Z$  boson masses induced by photon radiation correctly, it is necessary to consider photon transverse momenta as low as the calorimeter threshold of the detector, which is about 100 MeV. Subsequently, we therefore require

$$p_T(\gamma) > 0.1 \text{ GeV} \tag{10}$$

in all our calculations unless stated otherwise explicitly. The photon transverse momentum and pseudo-rapidity cuts are necessary to avoid soft singularities and collinear divergences associated with initial state radiation.

Since we are mostly interested in photon radiation in  $W$  and  $Z$  decays, we impose additional cuts on the di-lepton invariant mass,

$$75 \text{ GeV} < m(\ell\ell) < 105 \text{ GeV}, \tag{11}$$

and the transverse mass of the  $\ell\nu$  system,

$$65 \text{ GeV} < m_T(\ell\nu) < 100 \text{ GeV}. \tag{12}$$

CDF and DØ utilize similar cuts in their  $W$  mass analyses [16,17]. Events satisfying Eqs. (11) and (12) are called  $Z \rightarrow \ell^+\ell^-$  and  $W \rightarrow \ell\nu$  events, respectively, in the following.

To demonstrate that the multiconfiguration Monte Carlo approach we use yields accurate results both in the collinear region as well as for photons emitted at large angles, we show in Fig. 2 the differential cross section versus the separation between the two photons in the azimuthal angle-pseudorapidity plane,

$$\Delta R_{\gamma\gamma} = \sqrt{\Delta\phi_{\gamma\gamma}^2 + \Delta\eta_{\gamma\gamma}^2}. \tag{13}$$

The strong peak for small  $\Delta R_{\gamma\gamma}$  arises when both photons are emitted by the same charged lepton, and the photons are collinear with the lepton. The peak at  $\Delta R_{\gamma\gamma} \approx 3$  in  $\ell^+\ell^-\gamma\gamma$  production originates from Feynman diagrams where the photons are radiated off different leptons. Since photons do not couple to neutrinos, this peak is absent in  $\ell\nu\gamma\gamma$  production.

For electrons, the collinear peaks are significantly more pronounced than for muons. The difference in the differential cross sections for electrons and muons away from the collinear regions is entirely due to the different  $p_T$  and rapidity cuts imposed on these particles. The statistical fluctuations are quite uniform over the full range of  $\Delta R_{\gamma\gamma}$  values considered, indicating that the MCMC program distributes the generated events and their weights appropriately. Away from the collinear peaks, our calculation<sup>1</sup> agrees with that of Ref. [20] to better than 1%. In this region, conventional adaptive Monte Carlo routines such as VEGAS are sufficient in order to obtain a numerically stable result. The distributions of the separation between the photons and the charged lepton (leptons) are qualitatively very similar to the  $\Delta R_{\gamma\gamma}$  spectrum.

In Tables II and III, we list the fraction of  $W \rightarrow \ell\nu$  and  $Z \rightarrow \ell^+\ell^-$  events at the Tevatron which contain two photons as a function of the minimum photon transverse momentum. For comparison, we also list the event fractions containing one photon. Fractions are obtained by normalization with respect to the lowest order cross section within cuts. The results for  $\ell\nu\gamma$  and  $\ell^+\ell^-\gamma$  production are obtained using the calculation of Ref. [31]. No lepton-photon or photon-photon separation cuts are imposed.

Approximately 3% (1%) of all  $W \rightarrow e\nu$  ( $W \rightarrow \mu\nu$ ) events, and 14% (5%) of all  $Z \rightarrow e^+e^-$  ( $Z \rightarrow \mu^+\mu^-$ ) events, contain two photons with a minimum transverse momentum of  $p_T^{min}(\gamma) = 0.1$  GeV. Because of the mass singular logarithms associated with final state photon bremsstrahlung in the collinear limit, the fraction of  $W \rightarrow e\nu$  and  $Z \rightarrow e^+e^-$  events with two photons is more than a factor 3 larger than the corresponding fraction of  $W \rightarrow \mu\nu$  and  $Z \rightarrow \mu^+\mu^-$  events. In contrast to  $W$  events, both leptons can radiate photons in  $Z$  decays. As a result, the probability of  $Z \rightarrow \ell^+\ell^-$  events to radiate two photons is more than four times that of  $W \rightarrow \ell\nu$  events. For increasing  $p_T^{min}(\gamma)$ , the fraction of  $W$  and  $Z$  events

---

<sup>1</sup>Parton level FORTRAN programs for  $p\bar{p}^{(\pm)} \rightarrow \ell^\pm\nu\gamma\gamma$  and  $p\bar{p}^{(\pm)} \rightarrow \ell^+\ell^-\gamma\gamma$  which include the MCMC source code are available upon request from the authors.

containing photons drops quickly.

For small photon transverse momenta, the cross section is completely dominated by final state radiation. In this region, the fraction of events containing two photons,  $P_2$ , can be estimated using the simple formula [35]

$$P_2 = \frac{P_1^2}{2}, \quad (14)$$

where  $P_1$  is the fraction of events containing one photon. The results obtained using Eq. (14) are also listed in Tables II and III. For large values of  $p_T(\gamma)$ , the available phase space for final state radiation is strongly reduced by the transverse momentum cuts imposed on the leptons, and initial state radiation plays an increasingly important role. For  $p_T^{min}(\gamma) \geq 3$  GeV, Eq. (14) therefore becomes more and more inaccurate.

The large mass singular terms associated with final state bremsstrahlung result in a significant change in the shape of the  $m_T(\ell\cancel{p}_T)$  and the di-lepton invariant mass distributions. This is demonstrated in Fig. 3. Here we do not impose the di-lepton invariant mass cut and the  $\ell\nu$  transverse mass cut of Eqs. (11) and (12). In Fig. 3a we show the ratio of the  $\ell^+\ell^-\gamma\gamma$  and the lowest order  $\ell^+\ell^-$  cross section as a function of  $m(\ell\ell)$ . The cross section ratio is seen to vary rapidly. The dip at  $m(\ell\ell) = M_Z$  is a direct consequence of the Breit-Wigner resonance of the  $Z$  boson. Below the  $Z$  peak, the cross section ratio rises very sharply and in the region  $70 \text{ GeV} < m(ee) < 80 \text{ GeV}$ , the cross section ratio is of order one in the electron case. The dip located at  $m(\ell\ell) = M_Z$  and the substantially enhanced rate of events with two photons below the resonance peaks are caused by final state bremsstrahlung in events where the  $\ell^+\ell^-\gamma\gamma$  invariant mass is close to  $M_Z$ .

Fig. 3b displays the ratio of the  $\ell^+\nu\gamma\gamma$  and the  $\ell^+\nu$  cross section as a function of the  $\ell\nu$  transverse mass. Here the dip at  $m_T(\ell\cancel{p}_T) = M_W$  is due to the Jacobian peak in the  $\ell\nu$  transverse mass distribution. Because of the long tail of the lowest order  $m_T(\ell\cancel{p}_T)$  distribution below  $M_W$  and the fact that photons are not radiated by neutrinos, the enhancement in the  $\ell\nu\gamma\gamma$  to  $\ell\nu$  cross section ratio is less pronounced than that encountered in the  $\ell^+\ell^-$  case. In the region of large transverse masses,  $m_T(\ell\cancel{p}_T) > 100 \text{ GeV}$ , the shape of the transverse

mass distribution is sensitive to the  $W$  width. Fig. 3b shows that two photon radiation significantly modifies the shape of the  $m_T(\ell\nu)$  distribution in this region. This will directly influence the  $W$  width extracted by experiment.

The shape changes in the  $\ell\nu$  transverse mass and the di-lepton invariant mass distributions suggest that two photon radiation may have a non-negligible effect on the measured  $W$  and  $Z$  masses, and also on the  $W$  width extracted from the high transverse mass region. Since the shape change caused by two photon radiation in the distribution used to extract the mass is more pronounced in the  $Z$  case, the shift in the  $Z$  boson mass is expected to be considerably larger than the shift in  $M_W$ . For a realistic calculation of how  $\mathcal{O}(\alpha^2)$  corrections affect the  $W$  and  $Z$  resonance parameters, soft and virtual corrections and detector resolution effects need to be included.

We have not taken into account detector resolution effects or realistic lepton and photon identification requirements in the calculations presented in this Section. In particular, we have assumed that photons and leptons with arbitrary small opening angles can be discriminated. In practice, the finite resolution of the electromagnetic calorimeter makes it difficult to separate electrons and photons for small opening angles between their momentum vectors. Electron and photon four-momentum vectors are therefore recombined if their separation in the azimuthal angle-pseudorapidity plane is smaller than a critical value [16,17]. This eliminates the mass singular terms associated with final state photon radiation and thus may reduce the fraction of  $W$  and  $Z$  events with two photons significantly. Since muons are identified by hits in the muon chambers, the four momentum vectors of muons and photons are not combined for small opening angles. Instead, one frequently requires the photon energy to be below a threshold  $E_c$  in a cone around the muon. The mass singular logarithms thus survive in the muon case. The precise lepton identification requirements and their effects on the size of the EW corrections  $W$  and  $Z$  boson production are detector dependent.

#### IV. SUMMARY AND CONCLUSIONS

The mass of the  $W$  boson is one of the fundamental parameters of the SM and a precise measurement of  $M_W$  is an important objective for current experiments at LEP2 and future experiments at the Tevatron. A precise measurement of  $M_W$  helps to constrain the Higgs boson mass from radiative corrections. It will also provide restrictions on the parameters of the MSSM. In order to perform such a measurement at a hadron collider, it is crucial to fully control higher order QCD and EW corrections to  $W$  production. In a precision measurement of  $M_W$  in hadronic collisions, a simultaneous determination of the mass of the  $Z$  boson is required for calibration purposes. A detailed understanding of the QCD and electroweak corrections to  $Z$  boson production is therefore also necessary.

Recent calculations [14,15] have shown that the  $\mathcal{O}(\alpha)$  electroweak corrections to  $W$  and  $Z$  production have a significant impact on the weak boson masses extracted from experiment. The dominant contribution originates from final state photon radiation. The magnitude of the shift in  $M_W$  and  $M_Z$  induced by the  $\mathcal{O}(\alpha)$  corrections suggests that  $\mathcal{O}(\alpha^2)$  corrections may have an effect which cannot be ignored in future  $W$  mass measurements at the Tevatron. In this paper we have presented a calculation of the real  $\mathcal{O}(\alpha^2)$  photonic corrections to  $W$  and  $Z$  boson production in hadronic collisions. Our calculation is based on the full set of Feynman diagrams contributing to  $\ell^+\ell^-\gamma\gamma$  and  $\ell\nu\gamma\gamma$  production and includes finite lepton mass effects. In order to maintain gauge invariance in  $\ell\nu\gamma\gamma$  production, the  $W$  propagator and the  $WW\gamma$  and  $WW\gamma\gamma$  vertex functions are modified using the prescription given in Refs. [20] and [31].

In order to accurately determine the shift in the  $W$  and  $Z$  masses caused by photon radiation, the numerical calculation should be stable for arbitrarily small or large lepton - photon opening angles as well as for photon energies as small as the tower threshold of the electromagnetic calorimeter of the Tevatron experiments, which is of  $\mathcal{O}(100 \text{ MeV})$ . Due to the collinear and soft singularities present, this poses a challenge. Standard adaptive Monte Carlo integration routines such as VEGAS do not yield a stable result for processes



with a complicated peaking structure in the matrix elements, such as  $q\bar{q} \rightarrow \ell^+\ell^-\gamma\gamma$  and  $q\bar{q}' \rightarrow \ell\nu\gamma\gamma$ . To obtain numerically stable and accurate results in these cases, multi-channel Monte Carlo integration techniques are frequently used. This approach requires that the peaks in the matrix elements are analytically mapped. To calculate the cross sections for  $\ell^+\ell^-\gamma\gamma$  and  $\ell\nu\gamma\gamma$  production at hadron colliders, we developed a multiconfiguration Monte Carlo integration routine called MCMC which is based on a similar approach, adding the benefit of largely automizing the mapping of the peaks. MCMC thus can be used to calculate other processes with matrix elements exhibiting a complex set of peaks with almost no additional effort. The algorithm which is used in MCMC to map out the peaks is based on the Feynman diagrams which contribute to the process considered.

Imposing  $W$  and  $Z$  boson selection cuts on the final state leptons, we found that a significant fraction of weak boson events contains two photons. The probability for  $Z$  events to radiate two photons is almost a factor five larger than that for  $W$  events. For  $W \rightarrow \mu\nu$  and  $Z \rightarrow \mu^+\mu^-$  decays, the rate for two photon radiation is about a factor 3 smaller than the corresponding rate for decays with electrons in the final state. If the photon  $p_T$  is less than about 3 GeV, the fraction of  $W$  and  $Z$  events containing two photons can be estimated with an accuracy of 20% or better using a simple equation (see Eq. (14)).

Two photon radiation was also found to significantly alter the shapes of the  $Z$  boson resonance curve and the  $\ell\nu$  transverse mass distribution. The shift in the  $W$  and  $Z$  masses, and in the  $W$  width measured from the tail of the transverse mass distribution, caused by the  $\mathcal{O}(\alpha^2)$  real photon corrections may thus be non-negligible for future hadron collider experiments. For a realistic estimate of how strongly the  $\mathcal{O}(\alpha^2)$  corrections affect the  $W$  boson parameters extracted from experiment it is necessary to include the effects of soft and virtual corrections, as well as detector resolution effects. The calculation of  $\ell^+\ell^-\gamma\gamma$  and  $\ell\nu\gamma\gamma$  production presented in this paper thus only is the first step towards a more complete understanding of the  $\mathcal{O}(\alpha^2)$  electroweak corrections to  $W$  and  $Z$  production in hadronic collisions.

## ACKNOWLEDGMENTS

We would like to thank R. Brock, Y-K. Kim, M. Lancaster, D. Waters and D. Wood for stimulating discussions. One of us (U.B.) is grateful to the Fermilab Theory Group, where part of this work was carried out, for its generous hospitality. This work has been supported in part by DOE contract No. DE-FG02-91ER40677 and NSF grant PHY-9600770.

## REFERENCES

- [1] The LEP Collaborations, CERN-EP/99-15 (report, February 1999).
- [2] M. Acciarri *et al.* (L3 Collaboration), CERN-EP/99-80 (report, June 1999), to appear in Phys. Lett. **B**; G. Abbiendi *et al.* (OPAL Collaboration), CERN-EP/99-96 (report, July 1999), submitted to Eur. Phys. J. **C**; P. Bock *et al.* (The LEP working group for Higgs boson searches), ALEPH 99-081, DELPHI 99-142, L3 Note 2442, OPAL TN-614, paper contributed to the “*International Europhysics Conference on High Energy Physics*”, July 15 – 21, 1999, Tampere, Finland; J. Nielson *et al.*, (ALEPH Collaboration), hep-ex/9908016, paper contributed to the “*XIX International Symposium on Lepton and Photon Interactions at High Energies*”, Stanford, August 9 – 14, 1999.
- [3] M.S. Chanowitz, Phys. Rev. **D59**, 073005 (1999); G. D’Agostini and G. Degrassi, DFPD-99/TH/02 (preprint, February 1999); J. Mnich, talk given at the “*International Europhysics Conference on High Energy Physics*”, Tampere, Finland, July 15 – 21, 1999.
- [4] K. Hagiwara, D. Haidt and S. Matsumoto, Eur. Phys. J. **C2**, 95 (1998); G. Degrassi, P. Gambino, M. Passera, and A. Sirlin, Phys. Lett. **B418**, 209 (1998); G. Degrassi, Acta Phys. Polon. **B29**, 2683 (1998).
- [5] H. Aihara *et al.*, in “*Future Electroweak Physics at the Fermilab Tevatron: Report of the TEV\_2000 Study Group*”, eds. D. Amidei and R. Brock, FERMILAB-Pub-96/082, p. 63 (April 1996).
- [6] U. Baur and M. Demarteau, Proceedings of the Workshop “*New Directions in High Energy Physics*”, Snowmass, CO, June 25 – July 12, 1996, eds. D.G. Cassel, L. Trindle Gennari and R.H. Siemann, Vol. 1, p. 499.
- [7] M. Lancaster, FERMILAB-Conf-99/173-E (report, June 1999), to appear in the Proceedings of the “*XXXIVth Recontres de Moriond, Electroweak Interactions and Unified*

- Theories*”, Les Arcs, France, March 13 – 20, 1999; T. Dorigo, FERMILAB-Conf-99/155-E (report, April 1999), to appear in the Proceedings of the “XXXIVth Recontres de Moriond, QCD and Hadronic Interactions”, Les Arcs, France, March 20 – 27, 1999; T. Saeki, hep-ex/9906036 (report, June 1999), to appear in the Proceedings of the “XXXIVth Recontres de Moriond, QCD and Hadronic Interactions”, Les Arcs, France, March 20 – 27, 1999.
- [8] The LEP Collaborations, LEPEWWG/WW/99-01 (report, April 1999).
- [9] D. Partridge, Proceedings of the “XXIX International Conference on High Energy Physics”, Vancouver, B.C., Canada, 23 – 29 July, 1998, Vol. 1, p. 107; L. Demortier *et al.* (The Top Averaging Group), FERMILAB-TM-2084 (report, May 1999).
- [10] P. Chankowski *et al.*, Nucl. Phys. **B417**, 101 (1994); D. Garcia and J. Solá, Int. J. Mod. Phys. **A9**, 211 (1994); W. Hollik, KA-TP-23-1997 (September 1997), Proceedings of the “International Workshop on Quantum Effects in the MSSM”, Barcelona, Spain, September 9 – 13, 1997, p. 15.
- [11] D. Charlton, talk given at the “XIX International Symposium on Lepton and Photon Interactions at High Energies”, Stanford, August 9 – 14, 1999; A. Ballestrero *et al.*, in “Physics at LEP2”, eds. G. Altarelli, T. Sjostrand and F. Zwirner, CERN Yellow Report, CERN-96-01, Vol. 1, p. 141.
- [12] J.P. Marriner, Proceedings of the Workshop “New Directions in High Energy Physics”, Snowmass, CO, June 25 – July 12, 1996, eds. D.G. Cassel, L. Trindle Gennari and R.H. Siemann, Vol. 1, p. 78; P.P. Bagley *et al.*, Proceedings of the Workshop “New Directions in High Energy Physics”, Snowmass, CO, June 25 – July 12, 1996, eds. D.G. Cassel, L. Trindle Gennari and R.H. Siemann, Vol. 1, p. 134; D.A. Finley, J. Marriner and N.V. Mokhov, FERMILAB-Conf-96/408, presented at the “Conference on Charged Particle Accelerators”, Protvino, Russia, October 22 – 24, 1996; S. Holmes, FERMILAB-Conf-99/091, presented at “PAC99, Particle Accelerator Conference”, New

York, March 29 – April 2, 1999.

- [13] S. Keller and J. Womersley, Eur. Phys. J. **C5**, 249 (1998); A. Airapetian *et al.* (ATLAS Collaboration), “*ATLAS Detector and Physics Performance Technical Design Report, Vol. 2*”, CERN-LHCC-99-15, p. 547 (report, May 1999).
- [14] U. Baur, S. Keller and D. Wackerath, Phys. Rev. **D59**, 013002 (1999).
- [15] U. Baur, S. Keller and W.K. Sakumoto, Phys. Rev. **D57**, 199 (1998).
- [16] F. Abe *et al.* (CDF Collaboration), Phys. Rev. Lett. **75**, 11 (1995) and Phys. Rev. **D52**, 4784 (1995).
- [17] S. Abachi *et al.* (DØ Collaboration), Phys. Rev. Lett. **77**, 3309 (1996), B. Abbott *et al.* (DØ Collaboration), Phys. Rev. **D58**, 012002 (1998); *ibid.* **D58**, 092003 (1998); Phys. Rev. Lett. **80**, 3008 (1998); FERMILAB-Pub-99/237-E, hep-ex/9908057 (report, August 1999), submitted to Phys. Rev. **D**; FERMILAB-Pub-99/253-E, hep-ex/9909030 (report, September 1999), submitted to Phys. Rev. Lett.
- [18] F. Abe *et al.* (CDF Collaboration), Phys. Rev. Lett. **74**, 341 (1995).
- [19] E. Barberio, B. van Eijk, and Z. Was, Comput. Phys. Commun. **66**, 115 (1991); E. Barberio, and Z. Was, Comput. Phys. Commun. **79**, 291 (1994).
- [20] U. Baur *et al.*, Phys Rev. **D56**, 140 (1997).
- [21] G.P. Lepage, J. Comput. Phys. **27**, 192 (1978).
- [22] F.A. Berends, R. Pittau and R. Kleiss, Nucl. Phys. **B424**, 308 (1994); J. Hilgart, R. Kleiss and F. Le Diberder, Comput. Phys. Commun. **75**, 191 (1993); M. Skrzypek and Z. Was, CERN-TH/99-98 (preprint, April 1999); M. Skrzypek, S. Jadach, W. Placzek and Z. Was, Comput. Phys. Commun. **94**, 216 (1996).
- [23] R. Kleiss and R. Pittau, Comput. Phys. Commun. **83**, 141 (1994).

- [24] T. Stelzer, in preparation.
- [25] T. Stelzer and W.F. Long, *Comput. Phys. Commun.* **81**, 357 (1994).
- [26] T. Ohl, *Comput. Phys. Commun.* **120**, 13 (1999).
- [27] A. Pukhov *et al.*, hep-ph/9908288 (report, August 1999).
- [28] V.A. Ilyin, D.N. Kovalenko and A.E. Pukhov *Int. J. Mod. Phys.* **C7**, 761 (1996).
- [29] E.E. Boos *et al.*, *Int. J. Mod. Phys.* **C5**, 615 (1994) and references therein.
- [30] H. Murayama, I. Watanabe, and K. Hagiwara, KEK Report 91-11, 1992.
- [31] U. Baur and D. Zeppenfeld, *Phys. Rev. Lett.* **75**, 1002 (1995).
- [32] A.D. Martin, R.G. Roberts and W.J. Stirling, *Phys. Rev.* **D50**, 6734 (1994).
- [33] F. Abe *et al.* (CDF Collaboration), FERMILAB-Pub-96/390-E, (preprint, October 1996).
- [34] S. Abachi *et al.* (DØ Collaboration), FERMILAB-Pub-96/357-E (preprint, October 1996).
- [35] F. Bloch and A. Nordsieck, *Phys. Rev.* **D52**, 54 (1937); D.R. Yennie, S.C. Frautschi, and H. Suura, *Ann. Phys. (New York)* **13**, 379 (1961).

## TABLES

TABLE I. Integrated cross section for the process  $\nu_\mu\bar{\nu}_\mu \rightarrow e^+e^-\gamma\gamma$  at  $\sqrt{s} = 100$  GeV as a function of the electron mass for single and multi configuration adaptive Monte Carlo integration. A  $p_T > 10$  GeV cut is imposed on all final state particles. In all cases  $8 \times 100,000$  events are generated to set the grid, and  $5 \times 1$  million events for evaluating the integral.

electron mass	Multiconfiguration		Single configuration	
(GeV)	$\sigma$ (fb)	$\chi^2$	$\sigma$ (fb)	$\chi^2$
0.01	$88.4 \pm 0.8$	0.2	$48.9 \pm 3$	0.3
0.1	$46.34 \pm 0.08$	0.7	$36.5 \pm 2$	1.1
1.0	$17.14 \pm 0.03$	1.	$16.5 \pm 0.2$	0.7
10.0	$1.999 \pm 0.003$	0.3	$1.992 \pm 0.003$	0.2

TABLE II. Fraction of  $W \rightarrow e\nu$  and  $W \rightarrow \mu\nu$  events (in percent) containing one or two photons with a transverse momentum  $p_T(\gamma) > p_T^{min}(\gamma)$  at the Tevatron ( $p\bar{p}$  collisions at  $\sqrt{s} = 1.8$  TeV). Fractions are obtained with respect to the lowest order cross section. The cuts imposed are specified in the text. The relative statistical error on the event fractions from the Monte Carlo integration is approximately 1%.

$p_T^{min}(\gamma)$ (GeV)	$W \rightarrow e\nu\gamma$	$W \rightarrow e\nu\gamma\gamma$	$W \rightarrow e\nu\gamma\gamma$ [Eq. (14)]
0.1	23.9	3.05	2.86
0.3	17.3	1.56	1.50
1	10.4	0.53	0.54
3	4.82	0.09	0.12
10	0.56	$1.3 \times 10^{-3}$	$1.6 \times 10^{-3}$
$p_T^{min}(\gamma)$ (GeV)	$W \rightarrow \mu\nu\gamma$	$W \rightarrow \mu\nu\gamma\gamma$	$W \rightarrow \mu\nu\gamma\gamma$ [Eq. (14)]
0.1	13.5	0.99	0.91
0.3	9.65	0.48	0.47
1	5.74	0.17	0.16
3	2.65	$2.7 \times 10^{-2}$	$3.5 \times 10^{-2}$
10	0.33	$6.3 \times 10^{-4}$	$5.4 \times 10^{-4}$



TABLE III. Fraction of  $Z \rightarrow e^+e^-$  and  $Z \rightarrow \mu^+\mu^-$  events (in percent) containing one or two photons with a transverse momentum  $p_T(\gamma) > p_T^{min}(\gamma)$  at the Tevatron ( $p\bar{p}$  collisions at  $\sqrt{s} = 1.8$  TeV). Fractions are obtained with respect to the lowest order cross section. The cuts imposed are specified in the text. The relative statistical error on the event fractions from the Monte Carlo integration is approximately 1%.

$p_T^{min}(\gamma)$ (GeV)	$Z \rightarrow e^+e^-\gamma$	$Z \rightarrow e^+e^-\gamma\gamma$	$Z \rightarrow e^+e^-\gamma\gamma$ [Eq. (14)]
0.1	52.3	14.6	13.7
0.3	39.1	7.80	7.64
1	25.0	3.05	3.13
3	12.9	0.61	0.83
10	2.17	$1.3 \times 10^{-2}$	$2.4 \times 10^{-2}$
$p_T^{min}(\gamma)$ (GeV)	$Z \rightarrow \mu^+\mu^-\gamma$	$Z \rightarrow \mu^+\mu^-\gamma\gamma$	$Z \rightarrow \mu^+\mu^-\gamma\gamma$ [Eq. (14)]
0.1	31.2	4.76	4.87
0.3	23.8	2.67	2.83
1	15.4	1.07	1.19
3	8.19	0.25	0.34
10	1.62	$8.4 \times 10^{-3}$	$1.3 \times 10^{-2}$

# FIGURES

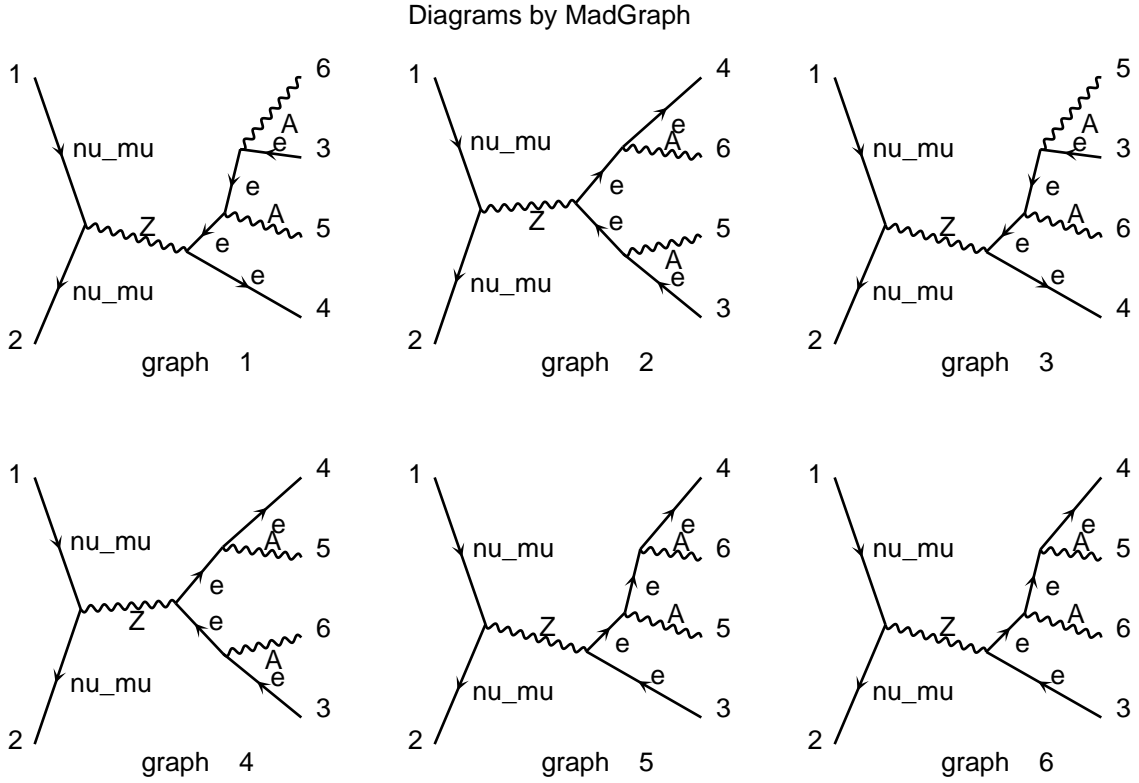


FIG. 1. The Feynman diagrams contributing to  $\nu_\mu \bar{\nu}_\mu \rightarrow e^+ e^- \gamma \gamma$  at tree level, as generated by MadGraph.  $A$  ( $Z$ ) represents a photon ( $Z$  boson),  $e$  an electron or positron, and  $\nu\_mu$  a muon neutrino,  $\nu_\mu$ .

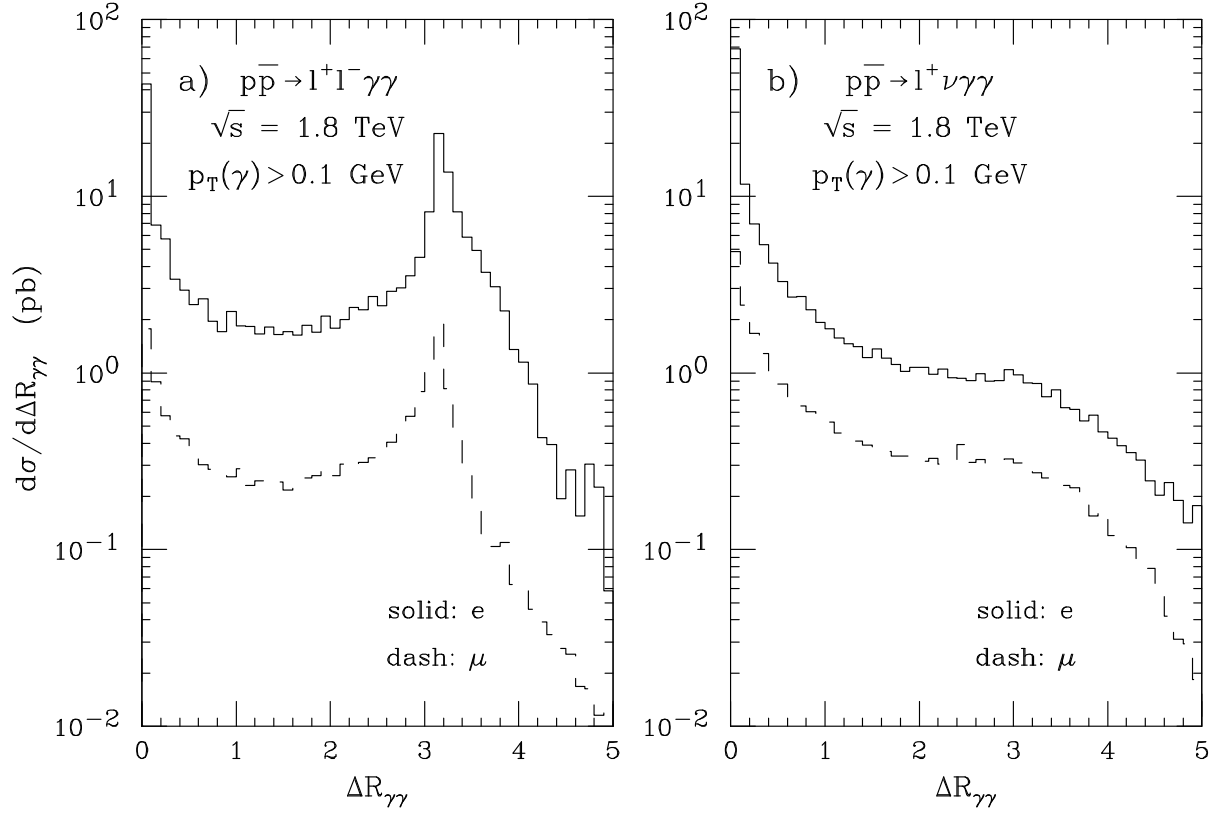


FIG. 2. The distribution of the separation between the two photons,  $\Delta R_{\gamma\gamma}$ , for a)  $p\bar{p} \rightarrow \ell^+ \ell^- \gamma\gamma$  and b)  $p\bar{p} \rightarrow \ell^+ \nu \gamma\gamma$  at  $\sqrt{s} = 1.8 \text{ TeV}$ . The solid and dashed histograms show the differential cross sections for electrons and muons, respectively. The cuts imposed are described in the text.

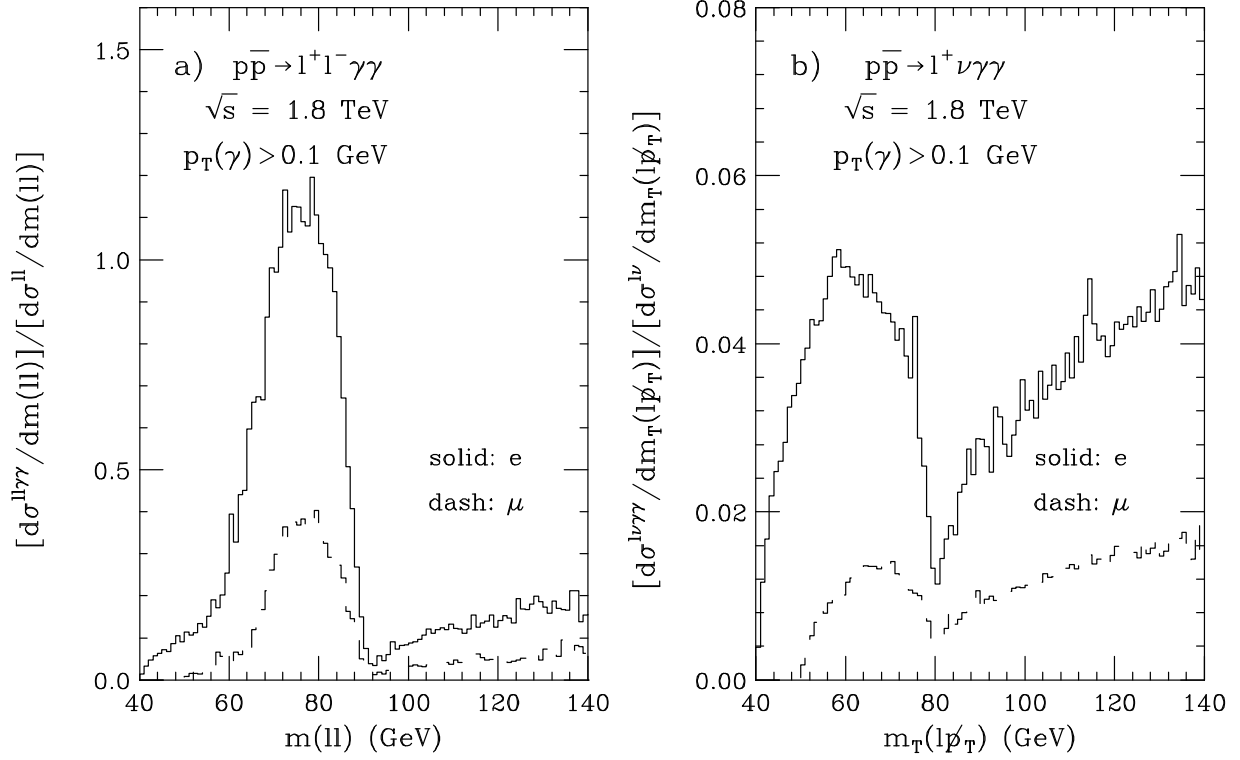


FIG. 3. Ratio of a) the  $p\bar{p} \rightarrow l^+l^-\gamma\gamma$  and the lowest order  $p\bar{p} \rightarrow l^+l^-$  cross sections as a function of the  $l^+l^-$  invariant mass, and b) the  $p\bar{p} \rightarrow l^+\nu\gamma\gamma$  and the lowest order  $p\bar{p} \rightarrow l^+\nu$  cross section versus  $m_T(l\not{p}_T)$  at  $\sqrt{s} = 1.8$  TeV. The solid and dashed histograms show the cross section ratios for electrons and muons, respectively. The cuts imposed are described in the text.